ORIGINAL PAPER

Fractal analysis of astrocytes in stroke and dementia

D. PIRICI[1)], L. MOGOANTĂ[1)], OTILIA MĂRGĂRITESCU[2)], IONICA PIRICI[3)], VALERICA TUDORICĂ[3)], MARIETA COCONU[3)]

[1)]*Department of Histology, University of Medicine and Pharmacy of Craiova*

[2)]*Department of Neurosurgery, Emergency County Hospital, Craiova*

[3)]*Department of Neurology University of Medicine and Pharmacy of Craiova*

Abstract

The varied morphological forms in which astrocytes occur in brain of ischemic/hemorrhagic stroke and Alzheimer's disease (AD) patients are complex and the mechanisms that drive their formation are not yet properly understood. Subjective differences can be described between these pathologies in what it concerns astrocyte implication, but these have not been yet subjected to a morphometrical quantification. Here we apply a fractal dimension (FD) analysis algorithm to differentiate both between fibrous, protoplasmatic and activated astroglia; but also between the three pathological conditions studied. Analyzing more than 1000 astroglia, we show here first that FD can clearly differentiate between the three morphological subtypes. Second, we describe resemblances of the FD values for ischemic and hemorrhagic lesions, and significant differences when these are compared to AD patients. These results are further discussed and integrated in what it regards the preferential regions proved to be affected in these conditions, and which parallels our results. This work illustrates that fractal dimension analysis of astroglia is a useful method for quantitatively describing gliosis in different pathologies, and that it may offer more insight into the pathogenesis of brain diseases.

***Keywords*:** fractal analysis, astrocytes, brain, stroke, hemorrhage, Alzheimer's disease.

Introduction

Astrocytes represent a ubiquitous type of glial cells that perform a variety of functions in the central nervous system (CNS). In fact, these are the most numerous type of cells encountered in the CNS, accounting for ten times the total number of neurons, or representing 25–50% of the whole brain volume [1–3].

Being highly active in regulating the brain parenchyma homeostasis, synaptic activity, regeneration, and immune- or injure-mediated cellular responses, they constitute an important line of defense against acute or chronic injuries [4–11].

Based on their morphological features on silver impregnation, these glial cells can be classified as resting protoplasmatic and fibrous astrocytes, or as activated astroglia.

Ischemic/hemorrhagic stroke and Alzheimer's disease (AD) represent two of the most aggressive forms of neurodegenerative brain diseases, being the second leading cause of death and respectively the most common form of dementia in all age groups [12, 13].

In response to all these brain injuries and neurodegeneration, astrocytes became activated and undergo a series of morphological and functional changes overall described as astrogliosis. With the proof that not only activation, but also transition between the resting forms may occur in disease, it became more and more accepted that glial reaction to disease might present no distinct specificity with respect to the etiology of the injury [14, 15].

Because of this continuous process of transformation and thus a relative high intra-group heterogeneity, classical morphometrical denominators such as areas, diameters, and perimeters do not suffice in differentiating astroglia responses [15].

To address this issue, for a more complete morphological description, scale-invariant parameters like fractal dimensions (FD) have been very useful in characterizing complex and non-regular objects [16].

The classical Euclidean geometric system has three dimensions, which are integers, an ideal line with no width has the dimension of one, a plane has the dimension of two, and a three-dimensional object has a dimension of three. FD of an object is a real number that expresses the morphological complexity and the inner self-similarity as measured on different scales, or simply put, a denominator of the space-filling properties of that object [16].

The closer this dimension is to the topological dimension of the space in which is considered, the greater is its space filling capacity. This concept is now widely used to describe many highly irregular normal and pathologically occurring patterns and processes like the bronchial tree ramification, the cerebral blood flow, tumor angiogenesis or the chromatin distribution in malignant cells [17–20].

In the present study, by applying FD as a morphological denominator for astroglia, we first aimed to test if the subjective classifications of astrocytes also have an objective basis; and second, we performed a detailed large-scale analysis of astrocyte FDs for different brain regions in hemorrhagic and ischemic strokes, as well as in AD cases.

To our knowledge, this is the first fractal analysis study on astrocytes to compare these frequent and aggressive brain pathologies.

Material and Methods

Tissue processing and immunohisto-chemistry

Formalin-fixed, paraffin-embedded archived brain tissue blocks were selected from ischemic (n=3) and hemorrhage stroke patients (n=3), sporadic AD patients (n=2), and age controls (n=2) (Table 1).

All the material is part of the brain bank currently under development as a result of the collaboration between the Departments of Histology, Pathology and Neurology, University of Craiova. For the stroke patients, tissue blocks were selected from the lesional sites and the peri-lesional areas. Equivalent regions were also included form all the other patients, including the AD and control cases. Six μm-thick sections were cut and processed for immunohistochemistry accordingly to producer recommendations (Table 2).

Table 1 – ***Patients included in the study***

Age [years]	Gender	Diagnostic
60	M	Striatal and pontine softening with hemorrhagic transformation. Temporal lesions are also noted.
46	F	Right hemisphere hemorrhage (temporal)
66	M	Bilateral frontal hemorrhage
52	M	Right hemisphere ischemic stroke (fronto-temporo-parietal)
63	F	Left hemisphere ischemic lesion (frontal), involving the basal ganglia
48	F	Left hemisphere ischemic stroke (fronto-temporal)
81	M	Sporadic Alzheimer's disease (AD)
68	F	Sporadic AD, bilateral frontal and basal ganglia ischemic stroke
85	M	Age control
76	M	Age control

Table 2 – ***The antibodies used in the study***

Name	Clonality	Epitope	Dilution	Retrieval	Source
4G8	Mouse, IgG1	Amino acids 17–24 of Aβ	1:30.000	Formic acid	Chemicon, Medicalkit, Craiova
Cleaved caspase 3	Rabbit, polyclonal	Activated caspase 3	1:100	0.1 M Citrate, pH 6	Cell Signaling, Medicalkit, Craiova
AT8	Mouse, IgG1	Tau protein phosphorilated at S202/T205	1:1000	–	NanuTec, Medicalkit, Craiova
CD34	Mouse, IgG1k	Vascular endotelium	1:100	0.1 M Citrate, pH 6	Dako, Medicalkit, Craiova
CD68	Mouse, IgG1k	Macrophages, monocytes	1:100	0.1 M Citrate, pH 6	Dako
GFAP	Rabbit, polyclonal	Astrocyte cytoskeleton	1:20.000	0.1 M Citrate, pH 6	Dako

Except GFAP, all other antibodies and routine Hematoxylin–Eosin stainings were utilized only in order to certify the pathologies to be studied. Briefly, after antigen retrieval, sections were cooled to room temperature and incubated for 30 minutes in a 1% hydrogen peroxide solution. The sections were next washed in PBS, followed by a final blocking step of 30 minutes in 1% skim milk. The primary antibodies were added, and the slides were incubated overnight at 4^0C. Next day, slides were washed and the signal amplified utilizing the Peroxidase–EnVision polymer-based species-specific secondary detection system (Dako, Medicalkit, Craiova, Romania), and then detected with 3,3'-diaminobenzidine (DAB) (Dako). All intermediate washing steps were done in 0.1 M PBS, pH 7.2, and all antibodies were diluted in PBS with 1% BSA (Sigma-Aldrich, Medicalkit, Craiova, Romania). All incubation times were kept constant for all the slides included in the present study. Finally, the slides were coversliped after a light Hematoxylin staining.

Image acquisition and processing

The sections were imaged with a Nikon Eclipse 90i microscope (Nikon, Apidrag, Bucharest, Romania) equipped with a 5-megapixel CCD camera and images of individual astrocytes were grabbed with 40× and 60× apochromatic objectives, as uncompressed TIF files utilizing the Image ProPlus software (Media Cybernetics). Six μm-thick sections were focused in different optical planes in order to resolve the finest details possible at this resolution. For each region that came in focus the software grabbed an image, and in the end, the "extended depth of field" algorithm generated a final image which recapitulated all the details of the cell (Figure 1, a–d). Cells without visible nuclei were rejected in this study. More than 100 cells were grabbed for each case in part, so more than 1000 images were analyzed in this study. Fifty clear-cut protoplasmatic, fibrous, and activated astrocytes were included in a pilot morphological study aimed to asses their characteristics as classes. Protoplasmatic astrocytes were identified as typical gray matter bushy cells with numerous short and ramified processes; fibrous astrocytes were typical white matter star shaped cells with long, thin and relatively non-ramified processes; and activated astroglia were recognized by a swelled cell body. Images were further processed with Image ProPlus. A Red-Green-Blue (RGB) signature of the DAB signal was created and all the images were automatically segmented keeping only the immunodetection signal. The masks obtained with this algorithm were then thresholded and saved as binary images containing the texture information for each astrocyte studied. Hole-filling and outline-detection

algorithms were next utilized to compensate for uneven cytoplasmatic staining pattern of the cells, and respectively to reduce the masks to the outlines of the binary silhouettes (Figure 1, e and f).

Due to the impossibility of following and resolving all cortex-wide long processes, radial glial cells were not considered in this study. Also, as subpial engorgement of glial limitans layer was a general observation in all pathologies described herein, and because the extremely dense fiber meshwork in this region did not allow a clear cut appearance to a certain cell body, the subpial reactivity was not considered in the study. Even though the number of cases available for this study was not very high, we obtained significant differences when making in-group and inter-group comparisons.

Fractal analysis

The binary images corresponding to the silhouettes or the outlines of the cells were then analyzed using the Image J software (Wayne Rasband, National Institutes of Health, Bethesda) together with the FracLac plug-in (A. Karperien – Charles Sturt University, Australia). FDs were calculated by the box-counting algorithm as the slope of the regression line for the log-log plot of the scanning box size and the count from a box counting scan (Figure 1, g and h).

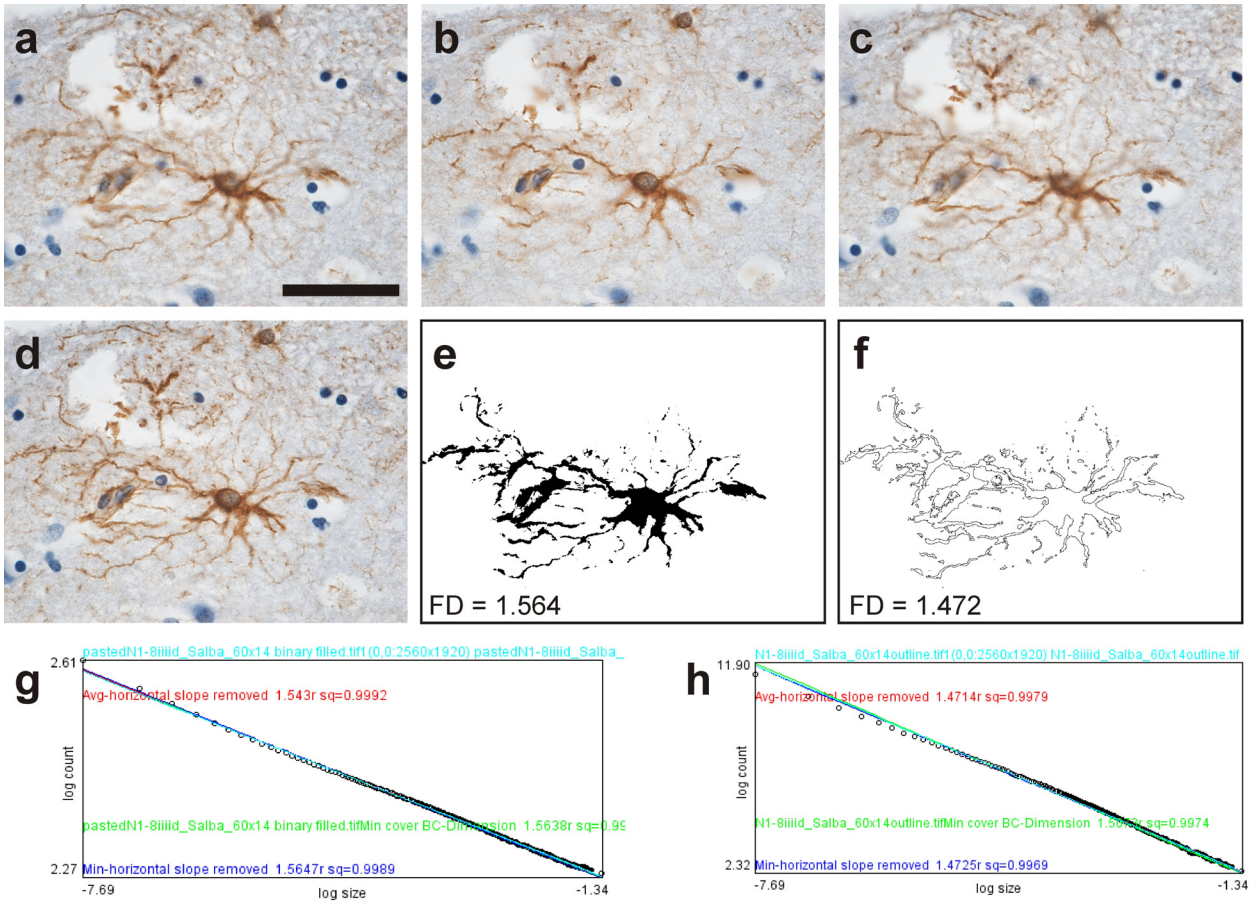

Figure 1 – ***Image processing algorithm for fractal analysis. Six µm-thick sections are focused in different optical planes with a 60× apochromatic objective in order to resolve the finest details possible at this resolution (a–c). After applying the "extended depth of field" algorithm, the resulting image captures all the details of the cell (d). The binarized silhouette was obtained after filling all the gaps in the inner mask of the image (e), and the outline contains only a pixel-thin edge of the binary silhouette (f). The fractal dimension is calculated for the binary silhouette (g) and the outline image (h), by the box-counting algorithm as the slope of the regression line for the log-log plot of the scanning box size and the count from a box-counting scan. Scales represent 50 µm.***

The software also delivers FD-values corrected for periods of no change in box count with changes in box size, and we further utilized this parameter to estimate the FD-values in our measurements. Lastly, all the raw data were exported and analyzed in Excel (Microsoft Corporation, Redmond, Washington, USA) or SPSS (SPSS Inc., Chicago, Illinois, USA). A one-way analysis of variance (ANOVA) was performed to compare average FD-values between different pathologies. A *t*-test was further utilized to compare FDs between different groups.

Results

Histopathological analysis

Larger intraparenchymal hemorrhages were readily identified on gross appearance of brain slices. There were widespread petechial hemorrhages that could be readily identified on the slides, with many engorged capillaries and evident vasculature discontinuities, with red blood cells extravasation (Figure 2). Cerebral edema and neuronal loss were also a common feature in and around the lesional sites. Organization of the

hemorrhage begun to be observed at its periphery, where microscopy showed collections of hemosiderin-laden macrophages. Activated astrocytes appeared from the earliest moments, and a yellow-brown lining due to perilesional gliosis and hemosiderin accumulation could be observed delineating already formed cavities. This corresponded to a dense belt of astrocytosis, which extended into the surrounding neuropil up to the glia limitans beneath the pial layer as anisomorphic gliosis.

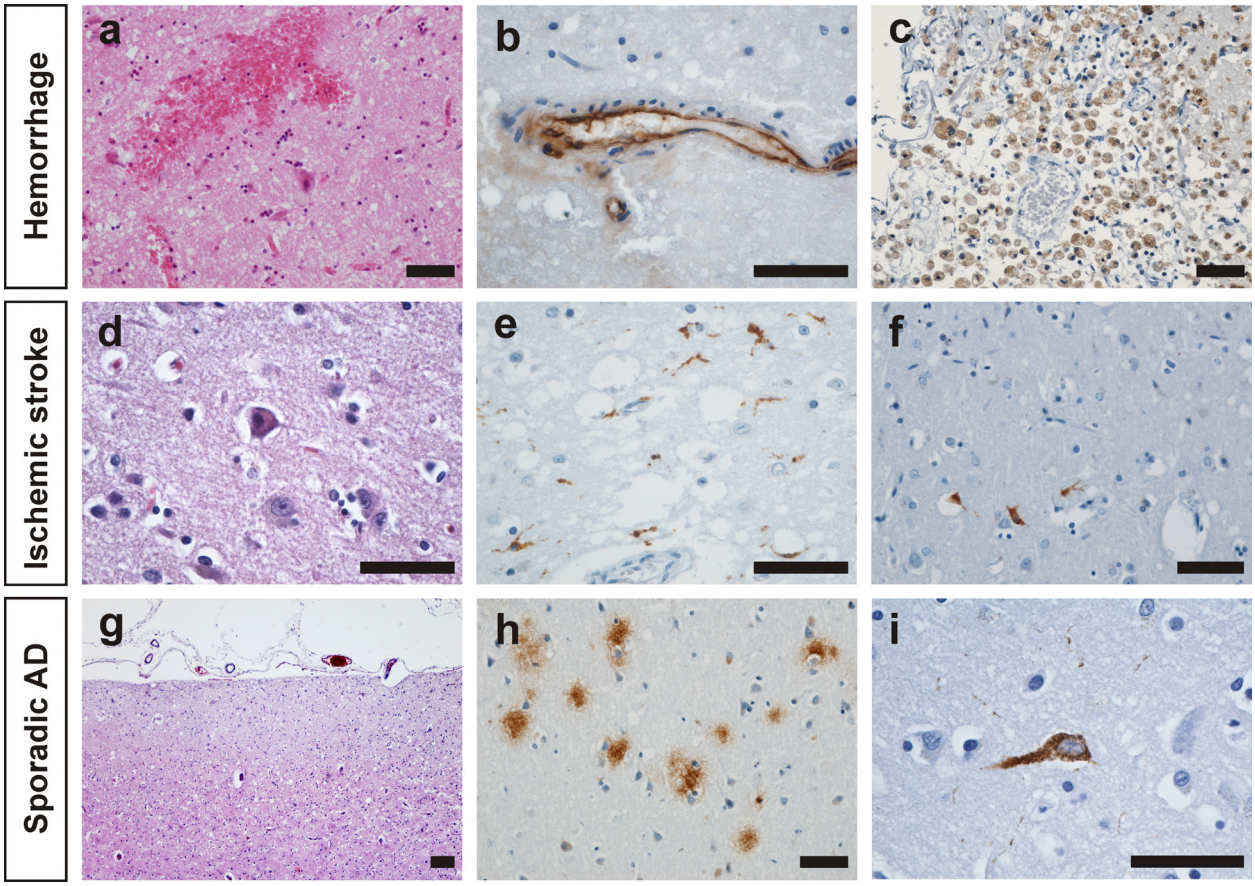

Figure 2 – ***Diagnostic confirmation for brain hemorrhages, ischemic strokes and Alzheimer's disease (AD). Petechial red blood cells extravasations (a), serum extravasation and endothelial discontinuity (b, immunohistochemistry for CD31), together with "foamy" macrophages (c) are characteristic for intraparenchymal hemorrhages. Red ischemic neurons (d), macrophage activation (e, immunohistochemistry for CD68), and apoptotic neurons (f, immunohistochemistry for activated caspase 3) characterize brain ischemia. Severe neuronal loss in the cortex (g), Aβ-amyloid containing plaques (h, immunohistochemistry for 4G8), and neurofibrillary tangles (i, immunohistochemistry for AT8) are characteristic features of AD. Scales represent 50 µm.***

Tissue pallor and softening were the first signs observed macroscopically for ischemic lesions, with accompanying hemorrhagic transformations in one of the cases. Microscopic analysis of areas with recent cerebral infarction revealed eosinophilic, hypoxic neurons in the affected areas, surrounded by tissue showing evidence of early cerebral edema with clear spaces around cells and vessels (Figure 2). Sometimes capillaries contained packed red blood cells because of passive hyperemia, and occasionally extravascular erythrocytes formed petechial hemorrhages. Later on, neuronal and glial loss became evident, and a spongious appearance of the parenchyma could be noted. Activated macrophages and monocytes were identified especially in the cores of the infarct. A staining for activated caspase-3 revealed sparse apoptotic neuronal figures, especially in the penumbra. Activated astrocytes had necrotic appearances in the central infracted regions, while classically plump, enlarged GFAP+-activated astrocytes could be identified not only in the penumbra, but also in remote brain areas and even contralateral hemispheres. In the core regions and in the penumbra, astrocytes could not be differentiated as fibrous or protoplasmatic anymore and this observation was made for both cortical and subcortical localizations. Anisomorphic astrocytosis predominated, with a general increased GFAP expression in the glia limitans, and the meshwork of fibers becoming denser as the glial scar formed in older ischemic lesions and around cavitation processes.

After the clinical confirmation, the two AD patients included in this study showed at necropsy a marked atrophy of the medial and lateral temporal lobes, with enlarged sulci and enlarged temporal horns of the lateral ventricles. There was no other obvious gross atrophy in other brain regions and substantia nigra was normally pigmented. One of the brains also showed evidence of small hemorrhages in both frontal lobes and in striatum. Microscopic examination revealed widespread neuronal loss in frontal, temporal and parietal regions, with accumulation of numerous amyloid deposits and neurofibrillary tangles (Figure 2). In both cases, there was no evidence for familial forms of AD.

Fractal characterization of the three morphological types of astrocytes

When selected astrocytes have been classified as fibrous, protoplasmatic and activated, the estimated silhouette FD-values for these groups showed a tendency for the protoplasmatic astrocytes to have the smallest FDs [1.43±0.04 (average±standard deviation)], fibrous astrocyte intermediate values (1.46±0.06), and activated astrocytes to have the highest FDs (1.50±0.05) (Figure 3). Because these cells have been pooled from all cases analyzed here, there was probably enough intra-group heterogeneity that impaired a clear-cut differentiation between them. Only protoplasmatic astrocytes could be shown to have significantly smaller values compared to activated astrocytes (p<0.05, t-test). The same hierarchy was evident when we analyzed the outlines of these cells: protoplasmatic (1.29±0.03), fibrous (1.34±0.02), and activated astrocytes (1.35±0.03) (Figure 3).

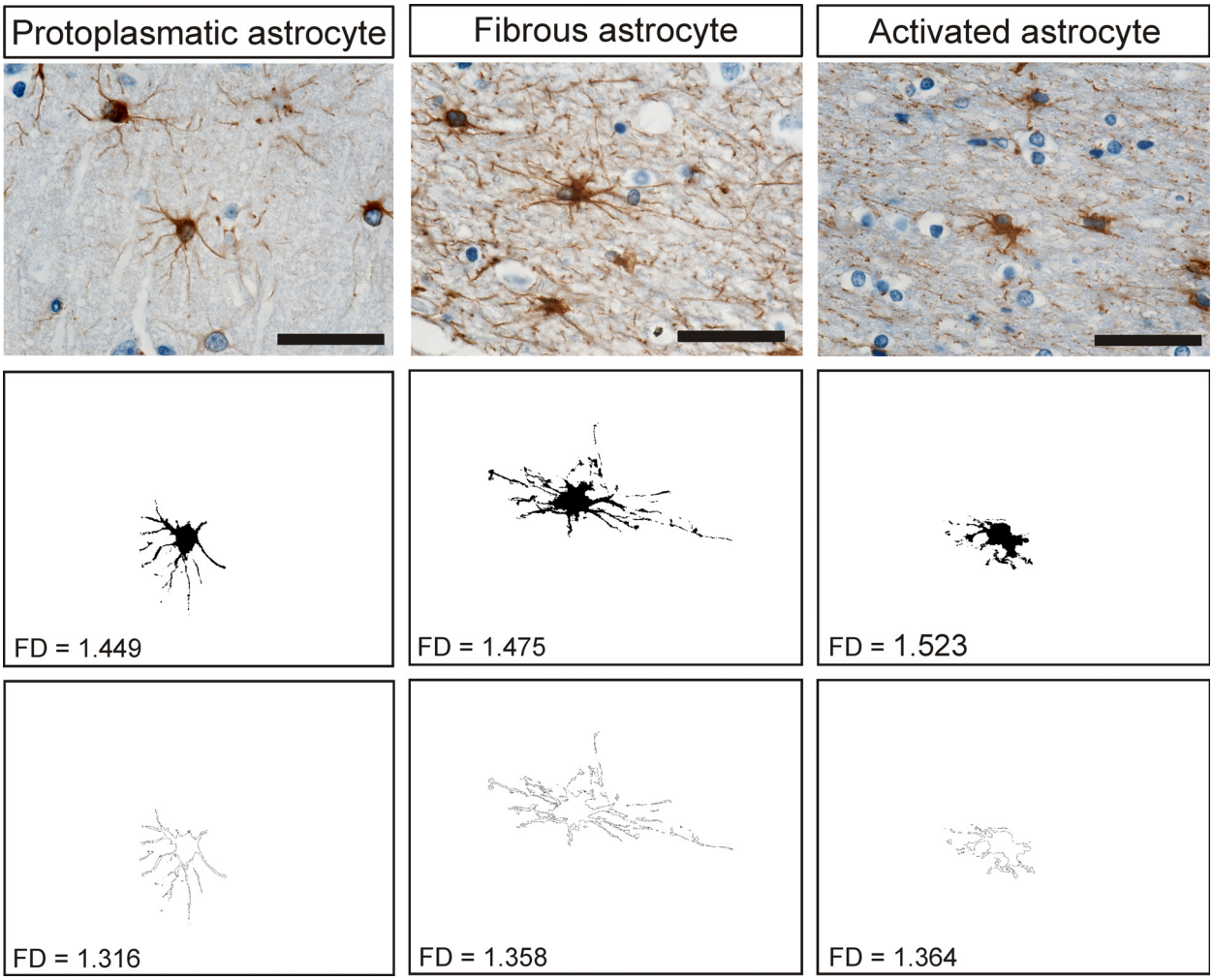

Figure 3 – ***Fractal analysis of the three main types of astrocytes. Grouped on columns are the original high-resolution images, the binary silhouettes and the outline masks together with the corresponding fractal dimension values.***

This classification showed that probably although apparently having a few more branching points on their processes, the arms of protoplasmatic astrocytes were smoother than those of the fibrous astrocytes, where relatively un-branched processes would span larger distances and would exhibit more sinuous trajectories. Although projections of the activated astrocytes were mostly short and blunt, the overall complexity of the perikarya proved these morphological types to have the highest FD values for both methods utilized.

Fractal astrocyte analysis in vascular brain lesions and dementia

Our main objective was to asses if a pooled type of analysis could differentiate between different brain regions and different pathologies.

For the hemorrhagic stroke, silhouette FDs could clearly differentiate between frontal, temporal and basal ganglia only for the white matter astroglia (one-way between types ANOVA, $F(2.76)=4.18$, p<0.05), with the temporal lobe having the highest values (1.61±0.09), the striatum having intermediate values (1.49±0.08), and frontal lobe the smallest FDs (1.40±0.01) (Figure 4a). Only in the temporal region, pooled cortical astrocytic reactivity (1.31±0.08) could be shown to be significantly lower than the subcortical reactivity (1.61±0.09) (p<0.001, t-test). There was a tendency for the temporal cortical FDs to be lesser than frontal cortical FDs, but this was non-significant on a closer view. On the paired analysis on the outlines of the cells, no difference could be recorded what so ever.

For the ischemic stroke group, silhouette FDs showed minimum values for temporal subcortical areas

(1.36±0.04) compared to frontal lobe (1.46±0.09) and striatum (1.50±0.09) ($p<0.05$, *t*-test) (Figure 4b). No difference could be recorded between frontal and striatal subcortical areas, but compared to the hemorrhagic strokes, here the temporal cortical FDs (1.34±0.11) showed significantly lower values compared to frontal cortical FDs (1.45±0.09) ($p<0.05$, *t*-test). For the outlines of the cells, subcortical FDs were different for all three studied regions (one-way between types ANOVA, $F(2.89)=4.25$, $p<0.05$).

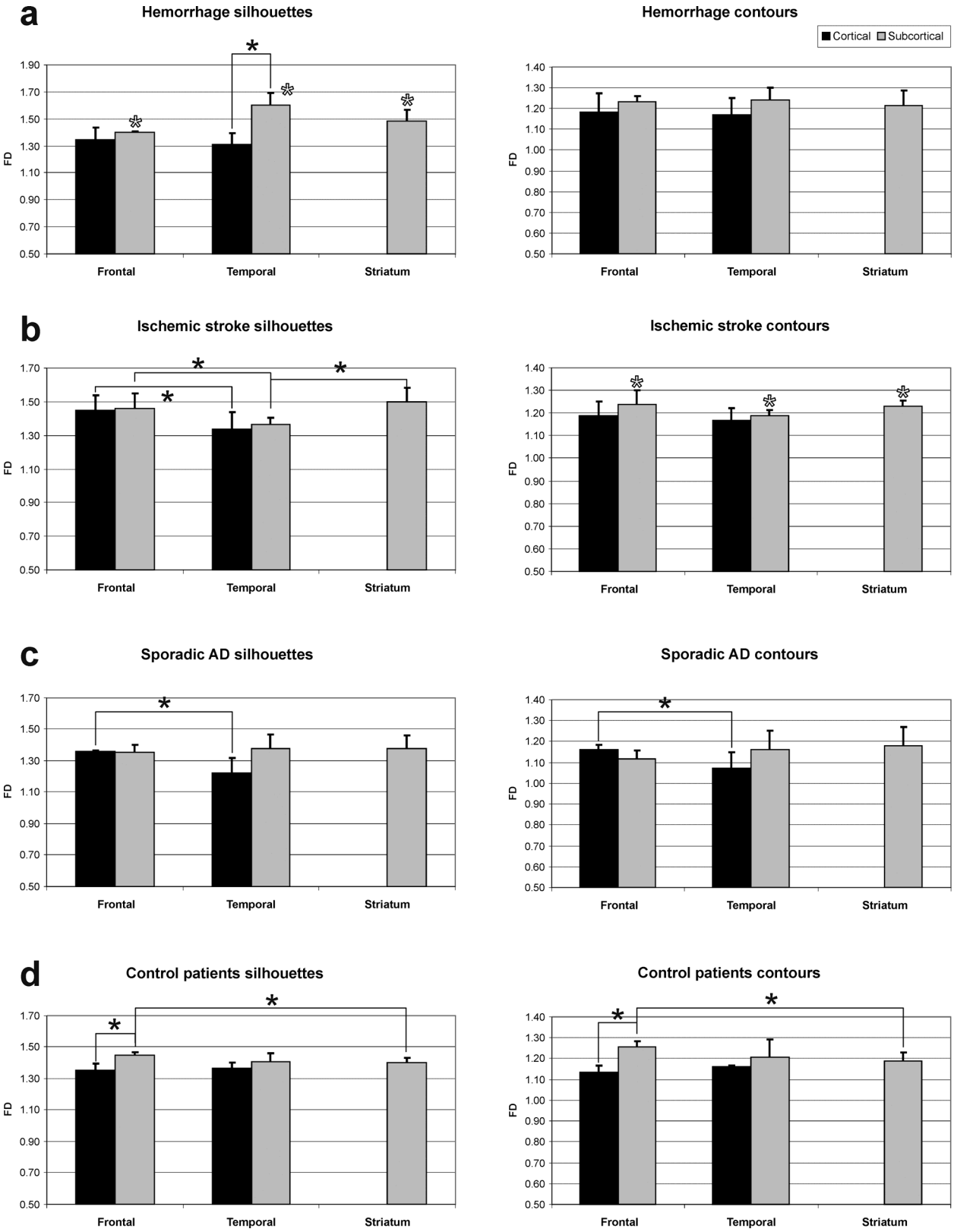

Figure 4 – ***Per pathology fractal morphometrical data. Astrocyte readings are pooled together to represent cortical and subcortical regions. Graphs represent average astrocyte fractal dimension values for binary silhouettes and contours, and are grouped on rows for hemorrhage (a), ischemic stroke (b), AD (c), and control cases (d). Full star represent significance on t-tests; empty stars represent significance on ANOVA-testing. Error bars represent standard deviation.***

For the sporadic AD group silhouette FDs showed again higher values for the frontal cortex (1.36±0.01) compared to the temporal cortex (1.38±0.02) (p<0.05, t-test) (Figure 4c). For the contour-based analysis, there was the same tendency for the frontal cortex (1.16±0.02) to have higher FDs compared to the temporal cortex (1.07±0.08) (p<0.05, t-test).

Measurements on control groups revealed frontal intra-group differences between cortical (1.36±0.04) and subcortical astroglia FDs (1.45±0.02) (p<0.05, t-test), as well as between frontal and striatal subcortical reactivities (1.40±0.03) (p<0.05, t-test) (Figure 4d). The same tendencies were noted for the outline measurements, with the frontal cortical FDs (1.13±0.03) being significantly lower than the subcortical morphologies (1.26±0.03) (p<0.05, t-test); and the frontal subcortical FDs being significantly larger than the striatal FDs (1.19±0.04) (p<0.05, t-test).

Finally, to have an integrated view of the whole pathological spectrum studied here, we pooled together cortical and subcortical regions and we compared inter-regional differences. For the frontal lobe, silhouette FDs were the highest for the ischemic stroke (1.46±0.06) and smallest for the AD pathology (1.36±0.02) (p<0.05, t-test) (Figure 5a). In the temporal lobe, AD FDs were still the smallest (1.29±0.03), while hemorrhage had the highest values (1.46±0.07), followed by controls (1.38±0.03) and ischemic stroke (1.35±0.05) (one-way between types ANOVA, F(3.78)=4.15, p<0.05). In striatum, hemorrhagic (1.49±0.07) and ischemic strokes (1.51±0.06) had significantly higher FDs compared to AD (1.38±0.04) and controls (1.41±0.03) (p<0.05, t-test). For the inter-lobe differences, only ischemic stroke FDs were differentiated, one-way between types ANOVA, F(2.87)=3.28, p<0.05. For the outlines analysis, AD FDs were again the smallest ones (1.14±0.03), and this difference was significant when comparing to hemorrhage (1.21±0.04) and ischemy (1.22±0.04) (p<0.05, t-test) (Figure 5b). The same tendency was recorded for the temporal lobe, AD values (1.12±0.04) being smaller than hemorrhage (1.21±0.02) and ischemy (1.18±0.02) (p<0.05, t-test).

In all pathologies studied, the number of patients and the homogeneity of the results did not allow any inter-gender demarcations.

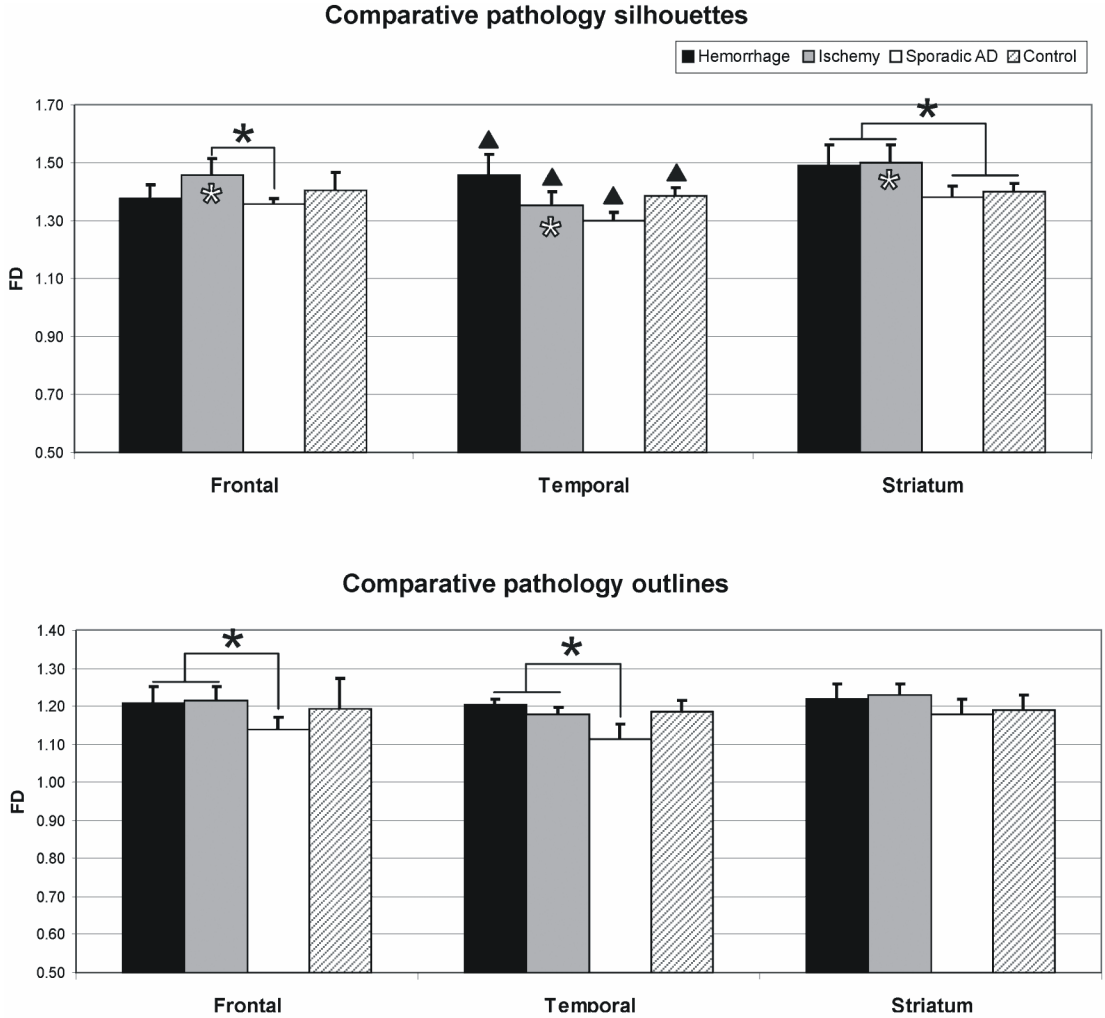

Figure 5 – ***Comparative fractal data pooled together for pathology and brain region. The data represent average astrocyte fractal dimension values on silhouette (a) and on outline (b) for the three studied brain regions (frontal, temporal, and striatum) and four pathological classes (hemorrhage, ischemy, sporadic AD, and control). Full star represent significance on t-tests; empty stars represent significance on inter-group ANOVA-testing; full triangles represent significance on intra-group ANOVA-testing. Error bars represent standard deviation.***

Discussion

The specific cellular architecture, function and immunoreactivity characterize astrocytes as a distinct class of glia. More and more data available today reveals the fact that astrocytes are not merely the structural scaffold of the brain, but that in fact they are actively involved in its metabolism. Structured as a net of highly branched cells interconnected via gap junctions and rich in receptors to most neurotransmitters, astrocytes regulate the brain interstitial fluid homeostasis of electrolytes, water, pH [4, 5], have been found to exhibit neurotrophic functions during development [21]; intervene in uptake and inactivation of neurotransmitters such as γ-amino butyric acid (GABA), dopamine or serotonin [6]; actively uptake serum albumin (and thus help in the resolution of brain edema) [22]; control the vascular tone [23]; inhibit or stimulate the adult CNS regeneration [7, 8]; modulate synaptic activity [9]; and mount immune- or injure-mediated responses [10, 11].

Generally characterized as star-shaped glial cells, examining silver sections impregnated with the technique of Golgi modified after Del Rio Hortega PD allows the differentiation of three main types of astrocytes [24]: (1) radial astroglia, with one long process located under pia matter, and other processes going oppositely into the gray matter, the nucleus being usually located near pia matter; (2) fibrous astrocytes, which are typical white matter star shaped cells with long, thin and relatively non-ramified processes; and (3) protoplasmatic astrocytes which are gray matter bushy cells with numerous short and ramified processes. Besides silver impregnation techniques, anti-GFAP and anti-S100 immunostainings are routinely used in diagnostic neuropathology as astrocyte markers. Anti-S100-staining allows the visualization of perikarya and especially the proximal part of their processes, while anti-GFAP staining usually allows a better detection of the cellular processes and to a lesser extent the perikarya. This was also the reasoning of choosing anti-GFAP immunostainings in our study, as a much simpler and selective alternative to special silver impregnations.

In response to brain injury and neurodegeneration, astrocytes undergo a series of morphological and functional changes that are overall described as astrogliosis. This reaction is mainly characterized by swelling of the cell body, presence of larger and thicker processes, with increasing GFAP-expression; the nucleus becomes more prominent and is usually displaced toward the periphery [15].

In studies on morphological changes, astroglia response to injuries is usually just described as focal/diffuse and isomorphic/anisomorphic gliosis. Classical quantification methods such as areas, diameters, and perimeters, did not yield significant results in objectively classifying astrogliosis, or even more, were not able to reveal differences between different pathologies [14, 15].

Fractal analysis is not new in neuropathology, previous other studies have shown its applicability in quantifying different types of activated microglia, in differentiating a variety of neuronal types and even look for interactions between astroglia and neurons [25–27].

Ischemic/hemorrhagic stroke and Alzheimer's disease (AD), on the other hand, represent two of the most aggressive forms of neurodegenerative brain diseases, as the second leading cause of death and respectively the most common form of dementia in all age groups [12, 13]. Given the importance of these pathologies, they have been the subject of the present work.

Hemorrhages in the brain are well-circumscribed lesions, and organization of a hemorrhage begins at its periphery, where microscopy reveals activated macrophages and astroglia. Astroglia surrounding the core of the intraparenchymal hemorrhage have been proved to become reactive and to overexpress remodeling factors like the matrix metalloproteinase-9 (MMP-9) [28]. A clear cut increase of the FD values for the temporal lobe in our study supports the idea of astroglia reactivity restricted to a precise location (surrounding the core of the lesion), compared to ischemic stroke where reaction is more generalized (see below). If we consider the fact that most of the small brain hemorrhages occur in the white matter, or in striatum [29], this completely explains the higher silhouette FD values for the subcortical region of the affected lobe and in basal ganglia.

Astrocyte swelling is among the first response to cerebral anoxia-ischemia [30, 31], and it seems that this process begins initially in the end-feets around the blood vessels, and then migrates towards the cell body [31]. Together with the abundant presence of activated astrocytes, this would explain the increased complexity and thus the higher silhouette FD values in the frontal lobes of our patients, as most had a frontal involvement compared to temporal lesions. When all data was pooled together, this FD value was in fact the highest among all studied pathologies. Also, it is now known that in penumbra, the surviving astrocytes undergo a process of hypertrophy [32], thus astroglial transformation becoming a generalized response to hypoxic lesions (and we observed in all cases a strong contralateral gliosis). Some authors suggested that the surviving astrocytes in the penumbra region of cerebral infarct may facilitate in restoring neuronal integrity by producing growth factors, cytokines, and extracellular matrix molecules, involved in repair and regenerative neuronal mechanisms [33]. Accordingly to this data, in our measurements FDs could not differentiate between cortical and subcortical gliosis.

Overall, in our hands silhouettes FDs brought the most significant differences compared to outline FDs, probably given the loss of lacunarity data in the second group.

Although it is known that astrocytes are generally more resistant to hypoxia compared to neurons, there is also a different sensitivity among astrocytes from different brain regions [34, 35], and this might as well modulate our results.

Alzheimer disease (AD) is the most frequent form of neurodegenerative disease. Besides amyloid plaques (mainly composed of the 4 kD β-amyloid peptide; Aβ)

and the tau neurofibrillary tangles (composed of hyperphosphorilated tau protein) [36, 37]; another commonly found pathological feature of AD is the abundance of astrogliosis in close proximity to neuritic dense plaques; that are typically the dense amyloid deposits that associate with neuronal loss and neuritic dystrophy [38]. Although other types of amyloid deposits do not usually induce a neuritic pathology and also no glial reaction, aggressive familial forms of AD have been described that associate diffuse neuritic pathology or cerebral amyloid angiopathy and an intense glial response [39, 40]. Aβ-peptide, besides its direct neurotoxic properties seem also to mediate astrocyte stimulation. *In vitro* studies revealed that exposure to Aβ-peptides leads to an alteration of the astrocytes' mitochrondial membrane potential, which results in the generation of free radicals, and subsequently contributes to an accelerated neuronal death [41]. On the morphological side, other studies found a preferential increase in the number of fibrous astrocytes [42, 43], with very long and relatively non-branched processes, which may explain the tendency of lower FD-values for AD-pathology in our study. Although the precise cause of this phenomenon in not known, when we re-visited the AD-slides, we indeed noticed that only very rare typically enlarged reactive astrocytes could be observed.

Although perivascular astrogliosis was a general finding in our AD patients, accordingly to literature data stating that striatum is less affected in AD [44], our results also show that FDs of the glial cells in AD do not differ from the ones present in the normal striate nuclei. As detailed above, this is in contrast to both hemorrhagic and ischemic strokes, which heavily involve striate nuclei.

However, both the mechanisms that trigger and regulate astrogliosis and the functional consequences of this activation for the surrounding neurons are not fully understood.

Thus, the present study reveals on one hand the resemblances between gliotic reaction in stroke and hemorrhage, and underlines on the other hand the major differences between these two diseases and AD.

Conclusions

First of all, to our knowledge, this is the first report to describe by fractal analysis the different astrocyte morphologies in these frequent neuropathological conditions.

Utilizing FD to characterize different types of astrocytic pathologies can indeed differentiate between classically recognized types of glial cells, and more, it can reveal some objective differences in the mechanisms that drive their pathogenic implications in different pathologies. These data also prompt towards introducing FD among the classical potential morpho-metrical classifiers that could be utilized as a set of observations in the training of an artificial neural network model that would greatly help in both tissue-oriented diagnostics and further research into the pathogenesis of astrogliosis.

Acknowledgements

This work was supported by the grant PNII/IDEI, CNCSIS–UEFISCU, ID 2188/2008.

References

[1] KIMELBERG H. K., NORENBERG M. D., *Astrocytes*, Scientific American, 1989, 260(4):66–72, 74, 76.

[2] MURÁNYI M., LACZA Z., [*Astrocytes in health and disease*], Orvosi Hetilap, 2007, 148(15):697–702.

[3] O'KUSKY J., COLONNIER M., *A laminar analysis of the number of neurons, glia, and synapses in the adult cortex (area 17) of adult macaque monkeys*, J Comp Neurol, 1982, 210(3):278–290.

[4] NEWMAN E. A., Glial cell regulation of extracellular potassium. In: KETTENMANN H., RANSOM B. R., *Neuroglia*, Oxford University Press, New York–Oxford, 1995, 717–731.

[5] DEITMER J. W., pH regulation. In: KETTENMANN H., RANSOM B. R., Neuroglia, Oxford University Press, New York–Oxford, 1995, 230–245.

[6] HENN F. A., HAMBERGER A., *Glial cell function: uptake of transmitter substances*, Proc Natl Acad Sci USA, 1971, 68(11):2686–2690.

[7] FITCH M. T., DOLLER C., COMBS C. K., LANDRETH G. E., SILVER J., *Cellular and molecular mechanisms of glial scarring and progressive cavitation: in vivo and in vitro analysis of inflammation-induced secondary injury after CNS trauma*, J Neurosci, 1999, 19(19):8182–8198.

[8] REILLY C. E., *Astrocytes instruct stem cells to differentiate into neurons*, J Neurol, 2002, 249(7):950–952.

[9] KUROSINSKI P., GÖTZ J., *Glial cells under physiologic and pathologic conditions*, Arch Neurol, 2002, 59(10):1524–1528.

[10] DIETRICH P. Y., WALKER P. R., SAAS P., *Death receptors on reactive astrocytes: a key role in the fine tuning of brain inflammation?*, Neurology, 2003, 60(4):548–554.

[11] MANDELL J. W., GOCAN N. C., VANDENBERG S. R., *Mechanical trauma induces rapid astroglial activation of ERK/MAP kinase: Evidence for a paracrine signal*, Glia, 2001, 34(4):283–295.

[12] ADAMS H. P. JR., *Guidelines for the management of patients with acute ischemic stroke: a synopsis. A Special Writing Group of the Stroke Council, American Heart Association*, Heart Dis Stroke, 1994, 3(6):407–411.

[13] KAWAS C. H., *Clinical practice. Early Alzheimer's disease*, N Engl J Med, 2003, 349(11):1056–1063.

[14] NIETO-SAMPEDRO M., SANETO R. P., DE VELLIS J., COTMAN C. W., *The control of glial populations in brain: changes in astrocyte mitogenic and morphogenic factors in response to injury*, Brain Res, 1985, 343(2):320–328.

[15] NORTON W. T., AQUINO D. A., HOZUMI I., CHIU F. C., BROSNAN C. F., *Quantitative aspects of reactive gliosis: a review*, Neurochem Res, 1992, 17(9):877–885.

[16] MANDELBROT B. B., *Stochastic models for the Earth's relief, the shape and the fractal dimension of the coastlines, and the number-area rule for islands*, Proc Natl Acad Sci USA, 1975, 72(10):3825–3828.

[17] MAUROY B., FILOCHE M., WEIBEL E. R., SAPOVAL B., *An optimal bronchial tree may be dangerous*, Nature, 2004, 427(6975):633–636.

[18] NAGAO M., MURASE K., KIKUCHI T., IKEDA M., NEBU A., FUKUHARA R., SUGAWARA Y., MIKI H., IKEZOE J., *Fractal analysis of cerebral blood flow distribution in Alzheimer's disease*, J Nucl Med, 2001, 42(10):1446–1450.

[19] SABO E., BOLTENKO A., SOVA Y., STEIN A., KLEINHAUS S., RESNICK M. B., *Microscopic analysis and significance of vascular architectural complexity in renal cell carcinoma*, Clin Cancer Res, 2001, 7(3):533–537.

[20] EINSTEIN A. J., WU H. S., SANCHEZ M., GIL J., *Fractal characterization of chromatin appearance for diagnosis in breast cytology*, J Pathol, 1998, 185(4):366–381.

[21] MENET V., GIMÉNEZ Y. R., SANDILLON F., PRIVAT A., *GFAP null astrocytes are a favorable substrate for neuronal survival and neurite growth*, Glia, 2000, 31(3):267–272.

[22] KLATZO I., CHUI E., FUJIWARA K., SPATZ M., *Resolution of vasogenic brain edema*, Adv Neurol, 1980, 28:359–373.

[23] REILLY C. E., *Astrocytes act as signal transducer in neuronal activation and cerebral arteriole vasodilation*, J Neurol, 2003, 250(3):384–386.
[24] DEL RIO-HORTEGA P. D., *Noticias de un nuevo y fácil método para la coloracion de la neuroglia y del tejido conjuntivo*, Trab Lab Invest Biol Univ Madrid, 1918, 15:367–378.
[25] SOLTYS Z., ZIAJA M., PAWLÍNSKI R., SETKOWICZ Z., JANECZKO K., *Morphology of reactive microglia in the injured cerebral cortex. Fractal analysis and complementary quantitative methods*, J Neurosci Res, 2001, 63(1):90–97.
[26] JELINEK H. F., FERNANDEZ E., *Neurons and fractals: how reliable and useful are calculations of fractal dimensions?*, J Neurosci Methods, 1998, 81(1–2):9–18.
[27] SCHAFFNER A. E., GHESQUIERE A., *The effect of type 1 astrocytes on neuronal complexity: a fractal analysis*, Methods, 2001, 24(4):323–329.
[28] TEJIMA E., ZHAO B. Q., TSUJI K., ROSELL A., VAN LEYEN K., GONZALEZ R. G., MONTANER J., WANG X., LO E. H., *Astrocytic induction of matrix metalloproteinase-9 and edema in brain hemorrhage*, J Cereb Blood Flow Metab, 2007, 27(3):460–468.
[29] REVESZ T., GHISO J., LASHLEY T., PLANT G., ROSTAGNO A., FRANGIONE B., HOLTON J. L.., *Cerebral amyloid angiopathies: a pathologic, biochemical, and genetic view*, J Neuropathol Exp Neurol, 2003, 62(9):885–898.
[30] GARCIA J. H., KALIMO H., KAMIJYO Y., TRUMP B. F., *Cellular events during partial cerebral ischemia. I. Electron microscopy of feline cerebral cortex after middle-cerebral-artery occlusion*, Virchows Arch B Cell Pathol, 1977, 25(3):191–206.
[31] PETITO C. K., BABIAK T., *Early proliferative changes in astrocytes in postischemic noninfarcted rat brain*, Ann Neurol, 1982, 11():510–518.
[32] NORENBERG M. D., The reactive astrocyte. In: ASCHNER M., COSTA L. G. (eds), *The role of glia in neurotoxicity*, 2nd edition, CRC Press, Boca Raton, Florida, 2005, 73–92.
[33] PANICKAR K. S., NORENBERG M. D., *Astrocytes in cerebral ischemic injury: morphological and general considerations*, Glia, 2005, 50(4):287–298.
[34] ZHAO G., FLAVIN M. P., *Differential sensitivity of rat hippocampal and cortical astrocytes to oxygen-glucose deprivation injury*, Neurosci Lett, 2000, 285(3):177–180.
[35] XU L., SAPOLSKY R. M., GIFFARD R. G., *Differential sensitivity of murine astrocytes and neurons from different brain regions to injury*, Exp Neurol, 2001, 169(2):416–424.
[36] ALZHEIMER A., *Über eine eigenartige erkrankung der Hinrinde*, Zentralblatt für Nervenheilkunde und Psychiatrie, 1907, 18:177–179.
[37] SELKOE D. J., *The cell biology of β-amyloid precursor protein and presenilin in Alzheimer's disease*, Trends Cell Biol, 1998, 8(11):447–453.
[38] KUMAR-SINGH S., CRAS P., WANG R., KROS J. M., VAN SWIETEN J., LÜBKE U., CEUTERICK C., SERNEELS S., VENNEKENS K., TIMMERMANS J. P., VAN MARCK E., MARTIN J. J., VAN DUIJN C. M., VAN BROECKHOVEN C., *Dense-core senile plaques in the Flemish variant of Alzheimer's disease are vasocentric*, Am J Pathol, 2002, 161(2):507–520.
[39] KUMAR-SINGH S., DE JONGHE C., CRUTS M., KLEINERT R., WANG R., MERCKEN M., DE STROOPER B., VANDERSTICHELE H., LÖFGREN A., VANDERHOEVEN I., BACKHOVENS H., VANMECHELEN E., KROISEL P. M., VAN BROECKHOVEN C., *Nonfibrillar diffuse amyloid deposition due to a gamma(42)-secretase site mutation points to an essential role for N-truncated A beta(42) in Alzheimer's disease*, Hum Mol Genet, 2000, 9(18):2589–2598.
[40] DERMAUT B., KUMAR-SINGH S., DE JONGHE C., CRUTS M., LÖFGREN A., LÜBKE U., CRAS P., DOM R., DE DEYN P. P., MARTIN J. J., VAN BROECKHOVEN C., *Cerebral amyloid angiopathy is a pathogenic lesion in Alzheimer's disease due to a novel presenilin 1 mutation*, Brain, 2001, 124(Pt 12):2383–2392.
[41] ABRAMOV A. Y., CANEVARI L., DUCHEN M. R., *Beta-amyloid peptides induce mitochondrial dysfunction and oxidative stress in astrocytes and death of neurons through activation of NADPH oxidase*, J Neurosci, 2004, 24(2):565–575.
[42] MANCARDI G. L., LIWNICZ B. H., MANDYBUR T. I., *Fibrous astrocytes in Alzheimer's disease and senile dementia of Alzheimer's type*, Acta Neuropathol, 1983, 61(1):76–80.
[43] SCHECHTER R., YEN S. H., TERRY R. D., *Fibrous astrocytes in senile dementia of the Alzheimer type*, J Neuropathol Exp Neurol, 1981, 40(2):95–101.
[44] DICKSON D. W., *The pathogenesis of senile plaques*, J Neuropathol Exp Neurol, 1997, 56(4):321–339.

Corresponding author
Daniel Pirici, Assistant, MD, PhD, Department of Histology, University of Medicine and Pharmacy of Craiova, 2–4 Petru Rareş Street, 200349 Craiova, Romania; Phone +40251–523 654, e-mail: daniel.pirici@yahoo.com

Received: May 15th, 2009

Accepted: August 5th, 2009